http://www.jstage.jst.go.jp/browse/biophysics

BIOPHYSICS

Vol. 6, pp. 1–11 (2010)
doi: 10.2142/biophysics.6.1

Actin oligomers at the initial stage of polymerization induced by increasing temperature at low ionic strength: Study with small-angle X-ray scattering

Takaaki Sato[1,6,*], Togo Shimozawa[2,7,*], Toshiko Fukasawa[1], Masako Ohtaki[2], Kenji Aramaki[3], Katsuzo Wakabayashi[4] and Shin'ichi Ishiwata[1,2,5]

[1]*Advanced Research Institute for Science and Engineering, Waseda University, 3-4-1 Okubo, Shinjuku-ku, Tokyo 169-8555, Japan*
[2]*Department of Physics, Faculty of Science and Engineering, Waseda University, 3-4-1 Okubo, Shinjuku-ku, Tokyo 169-8555, Japan*
[3]*Graduate School of Environment and Information Sciences, Yokohama National University, 79-7 Tokiwadai, Hodogaya-ku, Yokohama 240-8501, Japan*
[4]*Division of Biophysical Engineering, Graduate School of Engineering Science, Osaka University, Toyonaka, Osaka 560-8531, Japan*
[5]*Waseda Bioscience Research Institute in Singapore (WABIOS) , 11 Biopolis Way, #05-01/02 Helios, 138667 Singapore*
[6]*Present Address: International Young Researchers Empowerment Center, Shinshu University, 3-15-1 Tokida, Ueda 386-8567, Japan*
[7]*Present Address: Department of Physics, Graduate School of Science, The University of Tokyo, 7-3-1 Hongo, Bunkyo-ku, Tokyo 113-0033, Japan*

Received 13 November, 2009; accepted 17 November, 2009

Using small-angle X-ray scattering (SAXS), we have studied the initial stage (nucleation and oligomerization) of actin polymerization induced by raising temperature in a stepwise manner from 1°C to 30°C at low ionic strength (4.0 mg ml^{-1} actin in G-buffer). The SAXS experiments were started from the mono-disperse G-actin state, which was confirmed by comparing the scattering pattern in q- and real space with X-ray crystallographic data. We observed that the forward scattering intensity $I(q \to 0)$, used as an indicator for the extent of polymerization, began to increase at ~14°C for Mg-actin and ~20°C for Ca-actin, and this critical temperature did not depend on the nucleotide species, i.e., ATP or ADP. At the temperatures higher than ~20°C for Mg-actin and ~25°C for Ca-actin, the coherent reflection peak, which is attributed to the helical structure of F-actin, appeared. The pair-distance distribution functions, $p(r)$, corresponding to the frequency of vector lengths (r) within the molecule, were obtained by the indirect Fourier transformation (IFT) of the scattering curves, $I(q)$. Next, the size distributions of oligomers at each temperature were analyzed by fitting the experimentally obtained $p(r)$ with the theoretical $p(r)$ for the helical and linear oligomers (2–13mers) calculated based on the X-ray crystallographic data. We found that $p(r)$ at the initial stage of polymerization was well accounted for by the superposition of monomer, linear/helical dimers, and helical trimer, being independent of the type of divalent cations and nucleotides. These results suggest that the polymerization of actin in G-buffer induced by an increase in temperature proceeds via the elongation of the helical trimer, which supports, in a structurally resolved manner, a widely believed hypothesis that the polymerization nucleus is a helical trimer.

Key words: actin trimer, X-ray scattering, solution structure, oligomer distribution

Polymerization and depolymerization dynamics of actin are essential for various functions of eukaryotic cells, as actin filaments are a part of the cytoskeleton, which supports the cell movement and maintains cell shape[1,2]. These actin dynamics are controlled by many regulatory factors in cells[3,4]. However, it is nevertheless important to understand the detailed mechanism of actin polymerization, especially at its initial stage, in purified actin solution. The funda-

* These authors contributed equally to this work.
Corresponding author: Shin'ichi Ishiwata, Department of Physics, Faculty of Science and Engineering, Waseda University, 3-4-1 Okubo, Shinjuku-ku, Tokyo 169-8555, Japan. e-mail: ishiwata@waseda.jp

mental mechanism of actin polymerization (condensation phenomenon, being analogous to vapor-liquid equilibrium) was proposed by Oosawa and his colleagues[5], and this condensation mechanism has been confirmed by the extensive solution experiments including measurements of viscosity, spectroscopy, and light scattering. On the other hand, the double helix structure of actin filaments was directly observed by the electron microscopy[6], and the filament length distribution of polymerized actins under the steady state was confirmed to be exponential, as the theory predicted[7,8]. Moreover, polymerization and depolymerization dynamics at each end of individual actin filaments were directly observed in real time by total internal reflection fluorescence (TIRF) microscopy, which demonstrated that the theoretically predicted treadmilling mechanism[9], i.e., polymerization at the barbed-end and depolymerization at the pointed-end of actin filaments, did exist in the steady state[10]. Furthermore, the measurements with an advanced fluorescence microscopy technique called the photon counting histogram method suggested that in the steady state the linear and the helical oligomers coexist[11].

However, the structure and the length distribution of actin oligomers, which are expected to abundantly exist in the early stage of polymerization, are unknown. As for the polymerization nucleus, it was suggested to be composed of 3 or 4 monomers based on the time course analysis of the polymerization kinetics[12]. Surprisingly, there have, however, been no reports on the structure of the nucleus. The main reason complicating the identification of the nucleus is that it is not a stable complex, rather existing transiently, and, moreover, being on the order of several tens nanometers in size. Besides, in solution the nucleus coexists with oligomers of various sizes, as well as monomers. Small-angle X-ray scattering (SAXS) and small-angle neutron scattering (SANS) methods allow to determine the solution structure of such small-sized proteins. These scattering techniques have been used to investigate the solution structure of myosin S1 during ATP hydrolysis[13], actin at the initial stage of polymerization[14–16], the assembly processes of TMV[17] and microtubules[18], etc.

Here we used the SAXS method to study the polymerization process of actin prepared from rabbit white skeletal muscle. The application of SAXS to this subject is a real challenge, because the actin solution is a heterogeneous system composed of actin oligomers of various sizes. Polymerization kinetics are usually examined at some fixed actin concentration and a constant temperature by initiating the polymerization with the addition of salts, such as KCl and/or $MgCl_2$. Instead, here we examined a thermally activated polymerization process at low ionic strength (G-buffer), where at low temperatures the polymerization does not proceed. The polymerization was induced by raising the temperature in a stepwise manner, starting from ~1°C. We used a relatively high actin concentration, 4.0 mg ml^{-1}, and examined four different solvent conditions with different counterions and nucleotide species, i.e., Ca-ATP, Ca-ADP, Mg-ATP, and Mg-ADP bound forms. We have chosen these unusual conditions, aiming at the reliable detection of oligomers, which may exist at the initial stage of polymerization.

Materials and Methods

Preparation of proteins

All experimental procedures conformed to the "Guidelines for Proper Conduct of Animal Experiments", approved by the Science Council of Japan, and were performed according to the "Regulations for Animal Experimentation at Waseda University". Male white rabbits (2.0–2.5 kg) were anesthetized with pentobarbital (25 mg kg^{-1}), and actin was prepared from white skeletal muscle.

First, G-actin was prepared according to Spudich and Watt (1971)[19], except that tropomyosin-troponin complex was removed before preparing acetone powder, as previously described[20]. In order to prepare Ca-ATP-actin, Ca-ADP-actin, Mg-ATP-actin, and Mg-ADP-actin, purified G-actin was polymerized by adding 2 mM $MgCl_2$ or 2 mM $CaCl_2$ and 50 mM KCl, and after polymerization the solution was centrifuged at 411,000×g for 45 min at 8°C. The pellet was then dissolved in the solution containing 5 mM Tris-HCl (pH 8.0), 2 mM NaN_3, 50 μM $CaCl_2$ or $MgCl_2$, 0.1 mM ATP or ADP, and dialyzed against the same solvent overnight at 2°C, replacing the dialysis buffer at least twice. The same day the SAXS measurements were to be done, the G-actin solution had been centrifuged at 411,000×g for 20 min at 2°C to remove any aggregates, and the actin concentration was adjusted to 4.0 mg ml^{-1} by the dilution with the dialysis buffer. The concentration of G-actin was determined from the UV absorption (V-550, JASCO, Tokyo), assuming the molar extinction coefficient of 26,600 M^{-1} cm^{-1} at 290 nm.

SAXS measurements

We performed a series of SAXS experiments using a SAXSess camera (Anton Paar, Austria) attached to a PW3830 sealed-tube anode X-ray generator (PANalytical, Netherlands), which was operated at 40 kV and 50 mA. An equipped Göbel mirror, which consists of multilayers with laterally graded thickness, and a block collimator provided a focused monochromatic X-ray beam of Cu-K_α radiation (λ=0.1542 nm). A thermostated sample holder unit (TCS 120, Anton Paar) was used to control the sample temperature with an accuracy of 0.1°C. The samples were enclosed within a vacuum-tight thin quartz capillary with an outer diameter of 1 mm and a thickness of 10 μm, and the same capillary was used for all measurements including the buffer scattering to attain exactly the same scattering volume and background contribution. The 2D scattering pattern was recorded by an image plate (IP) detector (Cyclone, Perkin Elmer, USA) and integrated into the one-dimensional scattered intensities $I(q)$ as a function of scattering vector,

$q=(4\pi/\lambda)\sin(\theta/2)$, using SAXSQuant software (Anton Paar), where θ is the total scattering angle. All measured intensities were semi-automatically calibrated for transmission by normalizing a zero-q attenuated primary intensity to unity, by taking advantage of a semi-transparent beam stop. All $I(q)$ data were corrected for the background scattering from the capillary and the solvents, and the absolute scale calibration was made using water as a secondary standard.

Calculation of $p(r)$ and $p_c(r)$

Theoretically, $I(q)$ is given by Fourier transformation of the so-called pair-distance distribution function $p(r)$, i.e., the frequency of vector lengths, r, between small volume elements within the molecule, as

$$I(q)=4\pi\int_0^\infty p(r)\frac{\sin qr}{qr}dr \quad (1).$$

To extract intuitive real-space information via a virtually model-free routine, we used the indirect Fourier transformation (IFT) technique[21–23], which yielded the experimental $p(r)$ of actin aggregates. A model-free cross-section analysis of elongated structures of the protein aggregates is available when an axial length is at least three times longer than the cross-section diameter. The fluctuation profile of radial electron density, $\Delta\rho_c(r)$, is connected to the cross-sectional pair-distance distribution function, $p_c(r)$, as

$$p_c(r)=r\Delta\tilde{\rho}_c^2(r) \quad (2),$$

where $\tilde{}^2$ denotes the self-convolution.

Using an extended technique of IFT, $p_c(r)$ can be calculated directly from the experimental scattering intensity $I(q)$ for $q>2\pi/L$ (L: particle length) via

$$I(q)q=\pi LI_c(q)=2\pi^2L\int_0^\infty p_c(r)J_0(qr)dr \quad (3),$$

where $I_c(q)$ is the scattering intensity of cross-section and $J_0(qr)$ is the zeroth-order Bessel function.

Fitting of $p(r)$

When the actin solution contains various oligomers with different sizes, the observed SAXS data are considered to be the superposition of the scattering functions of these oligomers. Therefore, it should, in principle, be possible to deduce the oligomer distribution from the SAXS data by obtaining the best-fit combination of $p(r)$ for each oligomer taking into account the molecular weight ratio of each oligomer as a fitting parameter. However, since the determinative information about the structure of oligomers in solution does not exist, we introduced the following analytical method for the SAXS data; the model structure of each oligomer was produced from the reported crystallographic data of F-actin structure[24], and the theoretical $p(r)$ functions calculated for the constructed oligomer models were used to quantitatively describe the experimental $p(r)$ functions in solution.

We considered two types of model structures: one is the double-helix structure reported by Holmes and his colleagues, and the other is a linear structure constructed by removing one of the two long helical strands of F-actin. The linear actin filament has not yet been observed even by electron microscopy, although its existence was predicted by Oosawa and Kasai (1962)[5] and suggested by the photon counting analysis by Terada et al. (2007)[11].

Fitting of the modeled $p(r)$ to the experimentally observed distributions was performed with the *Levenberg-Marquardt* algorithm (SigmaPlot 11, Systat Software) to obtain the minimum value of the reduced error function, R^2, given by

$$R^2=\sum_{i=1}^{N}[p_{data}(r_i)-p_{fit}(r_i)]^2 \quad (4),$$

where $p_{data}(r_i)$ and $p_{fit}(r_i)$ stand for the values of the experimental data and the model function, respectively, at the ith distance, r_i. The iteration of the fitting procedure was stopped when the difference of R^2 between the two successive iterations became less than 10^{-4} (convergence condition). To cover a wide range of possible solutions with such many parameters, the fitting was automatically performed for the randomly chosen 100 different initial parameters.

Results and Discussion

Solution structure of actin before polymerization

Figure 1 shows a typical example of the SAXS experiments on G-actin, in which the data for Ca-ATP-actin at 1°C are presented. The scattering intensity $I(q)$ (Fig. 1a) is given as a double-logarithmic plot. The pair distance distribution function, $p(r)$ (Fig. 1b), was obtained by inverse Fourier transformation (IFT) of $I(q)$. We found that the experimental $p(r)$ for all G-actin species (Mg^{2+}, Ca^{2+}, ATP and ADP) in solution closely resembled $p(r)$ calculated from the crystallographic data of ADP-G-actin[25] without accounting for the contrast difference between hydrated and solvent water, which is shown by a solid line. On the other hand, it is known that the crystal structure of subdomain 2 of G-actin is slightly different between the ATP and ADP states[26]; besides, it was reported recently that the X-ray fiber diffraction of actin filaments showed that the angles between the subdomains 1, 2, and the subdomains 3, 4 in an actin monomer are slightly altered upon polymerization[27]. We calculated the $p(r)$ functions using their reported structural data, but they were indistinguishable from those of ATP-G-actin (data not shown), implying that little structural alterations, such as small conformational changes in the subdomain orientation, are not clearly detectable in the $p(r)$ analysis at the present resolution. Nevertheless, the data confirm the mono-dispersity of the solution within this resolution, implying that the G-actin solution at the initial stage of the following temperature-induced series of polymerization experiments was not contaminated with polymers.

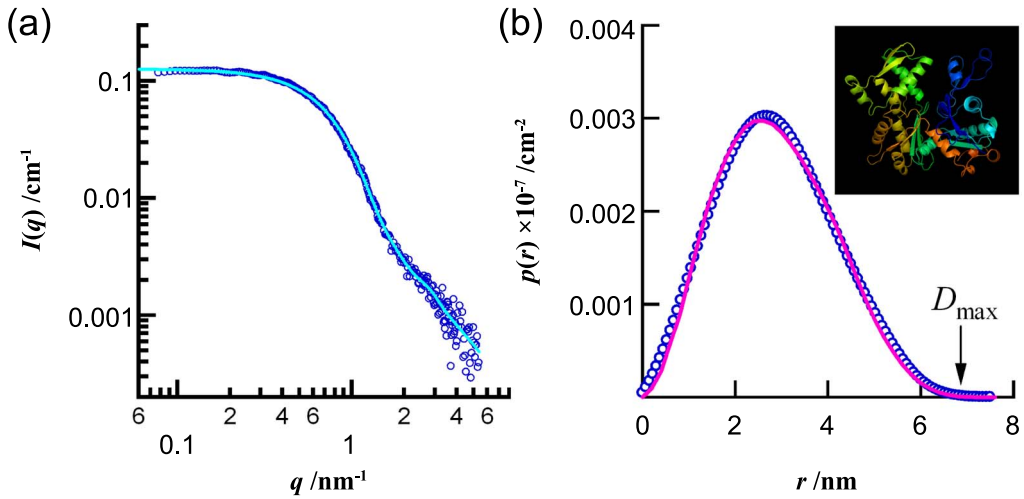

Figure 1 Particle characterization of G-actin by SAXS experiments.
(a), Scattering intensity $I(q)$, and (b), Corresponding pair-distance distribution function, $p(r)$, of G-actin (Ca-ATP) at 4°C. $p(r)$ refers to the spatial autocorrelation function of the electron density fluctuation of the protein in solution, which is obtained as inverse Fourier transformation of $I(q)$. In the inset of (b), the three-dimensional structure of G-actin[25] is presented by ribbon model. The pink solid curve shown in (b) represents (a) $p(r)$ function calculated from the crystallographic data of G-actin (PDB code 1J6Z).

SAXS data for temperature-induced polymerization of actin

Polymerization experiments have mostly been performed at a fixed temperature and protein concentration above critical by initiating the reaction with the added salts like KCl and/or $MgCl_2$. Instead, here we attempted to observe a thermally activated polymerization process with fixed protein and salt concentrations, by varying temperature, at a relatively high actin concentration (4.0 mg ml^{-1}) and four different solvent conditions with different counterions and nucleotide species, i.e., Ca-ATP, Ca-ADP, Mg-ATP, and Mg-ADP bound forms. Upon inducing the polymerization by raising temperature, the polymerization process can be viewed as a pseudo phase transition, each temperature step being regarded as a non-equilibrium, metastable phase. The polymerization was induced by raising temperature stepwise starting from 1°C to 30°C. A fixed low-salt condition chosen in this study is usually used for G-actin. The SAXS measurement at each temperature was done for 20 min after the incubation for 20 min.

Figure 2 shows the temperature dependence of the scattering intensity $I(q)$ and the corresponding $p(r)$ function in the presence of ATP with either Ca^{2+} (Figs. 2a, b) or Mg^{2+} (Figs. 2c, d). The forward scattering intensity, $I(q\rightarrow 0)$, abruptly increased at a certain temperature, demonstrating the initiation of polymerization. We call this temperature an onset temperature of polymerization T^* (see arrows in Figs. 2a, c). The reflection peak, which appeared distinctly at $q=1.15$ nm^{-1}, corresponds to the d-spacing of ca. 5.5 ($=2\pi/1.15$) nm. This can be recognized as a manifestation of orientationally averaged fiber diffraction peaks corresponding to the subunit axial translation, which are the so-called sixth- and seventh-layer lines known as the major characteristics of the established F-actin structure, i.e., a 13/6 symmetry. The peak at q~2.3 nm^{-1}, corresponding to the distance between the neighboring subunits along the F-actin filament, could also be seen, though somewhat vaguely.

Temperature dependence of polymerization of actin

We determined the average molecular weight of actin aggregates in solution, $\overline{M}_w(T)/M_w(T_0)$, as a function of temperature by referring to the relative zero-angle scattering intensity $I(q\rightarrow 0,T)/I(q\rightarrow 0,\ T_0)$, where T_0 is the initial temperature, at which the G-actin state of the sample was confirmed. The extrapolated zero-angle intensity, $I(q\rightarrow 0,T)$, was evaluated according to

$$I(q\rightarrow 0,T)=4\pi\int_0^\infty p(r)dr \qquad (5).$$

As shown in Fig. 3, the formation of actin oligomers upon increasing temperature is evident from $\overline{M}_w(T)/M_w(T_0)$. The circles and the squares in Fig. 3 indicate the non-fibrous and fibrous nature of actin polymers, respectively, in terms of the absence and presence of the fiber diffraction pattern in $I(q)$. We call the temperature at which the emergence of the fiber diffraction peak, a measure of the formation of F-actin, becomes apparent, a characteristic temperature, T_F. We anticipate that above T_F the actual length of the actin polymers, D_{max}, certainly exceeds the maximum resolution of our SAXS experiments, π/q_{min}~40 nm, where q_{min} is the accessible minimum scattering vector[23]. Simultaneously, the evaluation of $I(q\rightarrow 0,T)$ inevitability becomes less reliable, thereby giving perhaps underestimated average molecular weights.

The actin concentration, 4.0 mg ml^{-1}, used here is so high that actin aggregation proceeded even without ATP[5]. The

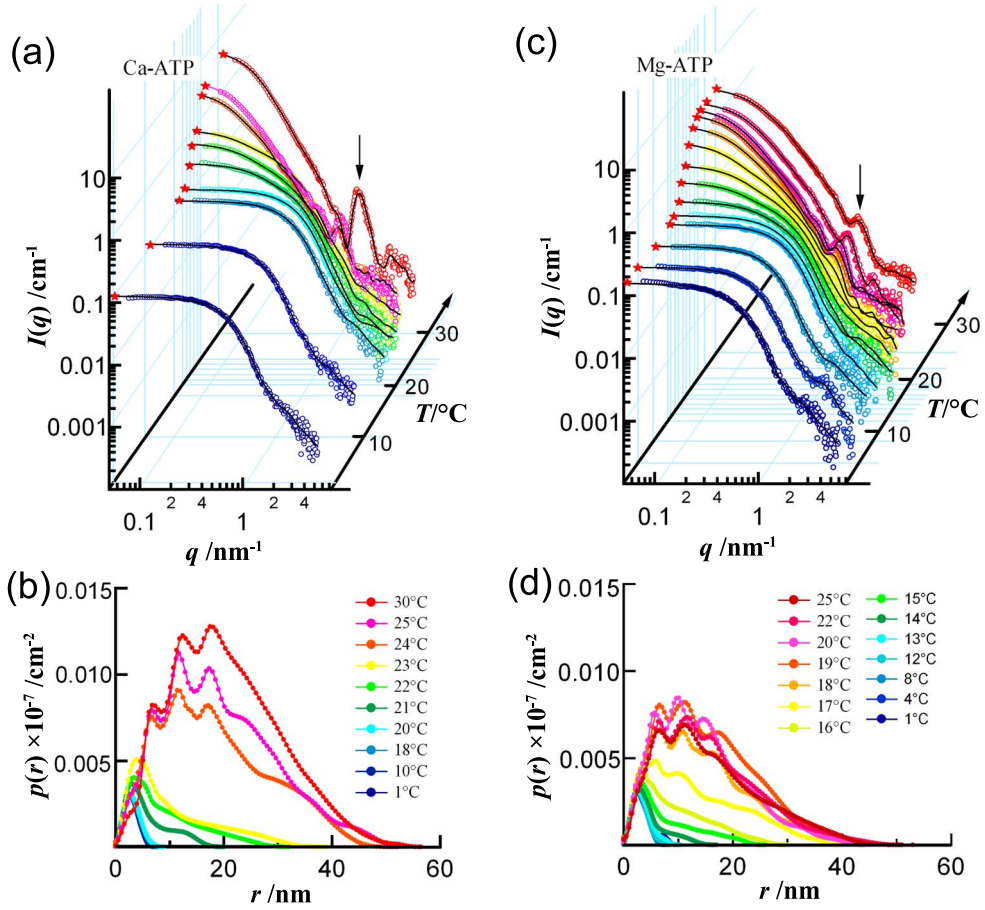

Figure 2 Temperature dependence of SAXS data for Ca-ATP and Mg-ATP actins.
(a) and (c): Scattering intensities $I(q)$, and (b) and (d): Corresponding pair-distance distribution functions, $p(r)$, for 4.0 mg ml^{-1} Ca-ATP (a), (c) and Mg-ATP (b), (d) actin solutions as a function of temperature. Arrows in (a) and (c) highlight the appearance of the orientationally averaged fiber reflection peak at q~1.15 nm^{-1} (see text).

effect of the divalent metal ions bound to the nucleotide binding site of G-actin is manifested by the different onset temperature T^* of polymerization. Under the present experimental conditions, T^* monitored by the onset of an increase in the forward intensity $I(q\rightarrow 0)$ was found to be essentially independent of the type of the ligand nucleotides (ATP or ADP), but affected by the divalent ion species (Ca^{2+} or Ma^{2+}), giving T^*~14°C and 18°C, respectively, for Mg and Ca forms (Fig. 2). This finding is clearly linked with the well-known fact that the replacement of Ca^{2+} with Mg^{2+} significantly promotes the formation of nucleus[28–30].

However, it is interesting to note that the critical temperature for polymerization was independent of the nucleotide species; the result seems to be inconsistent with the well-known fact that the critical actin concentration for polymerization is much higher for ATP-actin[20,31]. This apparent contradiction may be attributed to the new polymerization conditions employed in the present study. One possible explanation may be that the structure of ATP-G-actin is similar to that of ADP-G-actin at low ionic strength, as far as the nucleation is concerned.

Real space information on the structure of actin oligomers based on the experimental $p(r)$ profiles

Further insights into transient structures of actin oligomers can be gained from $p(r)$ obtained as an output of IFT of the $I(q)$ data, which provides virtually model-free real space information on the self-assembled structures. With increasing temperature above T^*, the high-r tail of $p(r)$ rapidly extended (Fig. 2b, d), showing the formation of longer polymers. This tendency maintained until the maximum length, D_{max}, of the aggregates, indicated by the r-value where $p(r)$ converges to zero, reached ca. 30–35 nm. As soon as F-actin was formed, the emerging fiber diffraction peak in $I(q)$, which is transcribed into real space, strongly affected the shape of $p(r)$, creating a 5.5 nm equidistant peak sequence on $p(r)$.

Theoretical $p(r)$ calculated based on the crystallographic data of actin polymers

For a quantitative analysis, we attempted to compare the $p(r)$ functions in solution obtained by SAXS with the theoretical distributions calculated from the crystal structures of

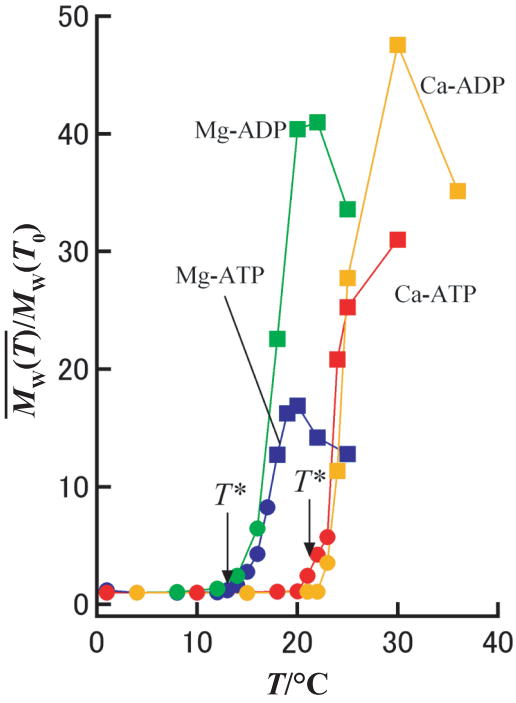

Figure 3 Effect of temperature on polymerization of actin with different divalent cations and nucleotides.

Relative average molecular weight of actin aggregates in solution, $\overline{M}_w(T)/M_w(T_0)$, plotted as a function of temperature determined from an extrapolated zero-angle scattering intensity $I(q\rightarrow 0)$ is shown for Ca-ATP-actin (red), Ca-ADP-actin (orange), Mg-ATP-actin (blue), and Mg-ADP-actin (green). Circles and squares indicate, respectively, the non-fibrous and fibrous nature of actin oligomers judged from the absence or presence of the fiber reflection pattern in $I(q)$. The temperature T^*, at which polymerization starts, depends not on the nucleotide state, but on the divalent cation species.

actin filaments. The oligomer models were constructed from the F-actin structure, which was derived by fitting the atomic structure of G-actin determined from the X-ray crystallography to the X-ray fiber diffraction data from the oriented sols of F-actin[24]. Using the PDB coordinates (ftp://149.217.48.3/pub/holmes/pdb/crystal_structure_actin_helix.pdb), we calculated $p(r)$ functions for helical polymers (H) ranging from a dimer (H2) up to a 13mer (H13) (Fig. 4a). We also calculated the $p(r)$s for the linear actin polymers (L) ranging from a dimer (L2) to a 7mer (L7) (Fig. 4b). Since the linear form has not been established yet, the linear polymers were created by simply removing one of the two major helical strands as shown in Fig. 4c.

The solution structure of actin at the initial stage of polymerization

Since actin (pI=5.4) carries a net negative charge of approximately 5 electron charges at physiological pH, the orientationally averaged net electrostatic interaction between the proteins must be repulsive[32]. Thus, actin aggregation must be considered to occur via a site-specific interaction between the proteins. The knowledge about actin nucleation is of remarkable importance for the understanding of many biological processes mediated by actin polymerization-depolymerization dynamics. The nucleation must involve

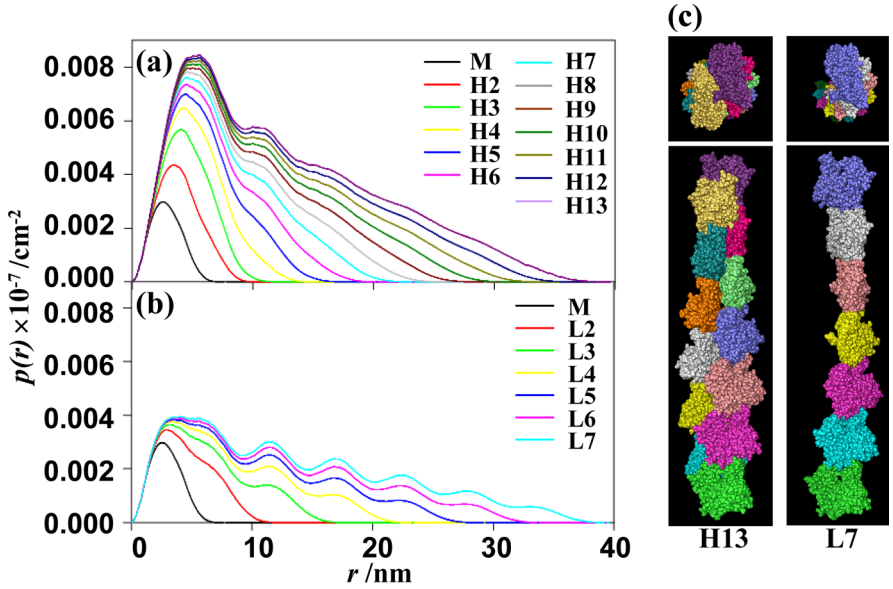

Figure 4 $p(r)$ functions simulated from the model structures of helical and linear polymers.

(a), $p(r)$ simulated from the crystal structures of a helical polymer (dimer (H2)~13mer (H13)) and a monomer. (b), $p(r)$ simulated from the crystal structures of a linear polymer (dimer (L2)~7mer (L7)) and a monomer. The actin concentration was 4.0 mg ml^{-1}. (c), Three-dimensional structures of various actin aggregates: a helical 13mer (H13) (left) and an assumed linear 7mer (L7) (right). The model structure was obtained from PDB data of the Holmes' actin filament model[24]. The structure of a linear polymer was produced from the helical structure (see text).

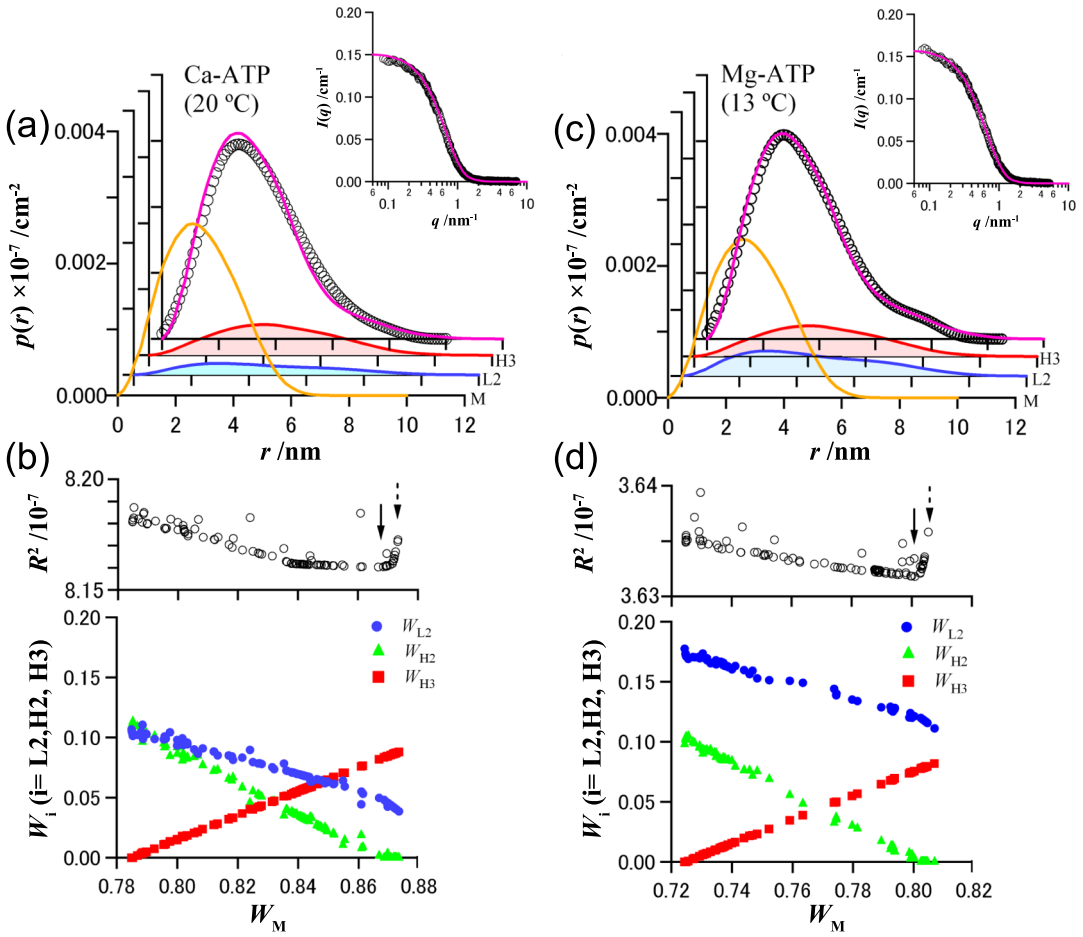

Figure 5 Structural characterization of actin aggregates at the initial stage of polymerization.

Analysis of the experimental $p(r)$ at T~T* assuming the mixture model of a monomer (M), a linear dimer (L2), a helical dimer (H2), and a helical trimer (H3): (a), Ca-ATP at 20°C, and (b), Mg-ATP at 13°C. (b) and (d), The examined 100 parameter sets for different weight fractions of H2, L2, and H3 (W_{H2}, W_{L2} and W_{H3}) and their R^2 values obtained as a function of the monomer weight fraction (W_M). (a) and (c), The experimental $p(r)$ (open black circles) and the fitting curve (pink solid line) based on the superposition of the simulated $p(r)$ functions of M, L2, and H3 (sequential solid lines, orange, blue and red, respectively). In the insets of the panels (a) and (c), the experimental scattering intensity $I(q)$ and the fitting curve using $I(q)$ simulated from the crystal data are shown. This confirms simultaneous successful description of the scattering data in both q-space and a real space. Solid arrows indicate the minimal values of R^2. Dashed arrows indicate R^2 for the parameter sets that correspond to the panels (a) and (c).

self-organization of actin monomers, serving as the building blocks of a filament, into a stable polymerization nucleus. It is generally believed that a nucleus is a helical trimer, because this is the smallest complex that essentially involves all basic intermolecular interactions between the neighboring monomers in the filamentous form. Quite surprisingly, however, there exists no direct supporting structural evidence so far. Aiming at testing this hypothesis on the nucleus structure, we tried to structurally resolve the solution structure of actin at the initial stage of polymerization, i.e., Ca-ATP at 20°C and Mg-ATP at 13°C, using a mixture model implying the coexistence of a monomer (M), a linear dimer (L2), a helical dimer (H2), and a helical trimer (H3). In this analysis, a linear trimer and the aggregates larger than a tetramer were not considered, judging from D_{max} of the experimental $p(r)$.

As shown in Figure 5, we found that $p(r)$ of the initial stage of polymerization (T~T*) was well accounted for by the superposition of either M, L2, H2, and H3, or M, L2, and H3 with a smaller number of the adjustable parameters. A pathway of the helical trimer (H3) formation, namely, whether it is M→L2/H2→H3 or M→L2→H3, cannot be decisively established from the present analysis. Nevertheless, we infer that M→L2→H3 may be a more plausible nucleation pathway, because the weight fraction of L2 is always greater than that of H2, and, as highlighted by solid arrows in Fig. 5, the minimum of R^2 was attained at the distribution that was very close to M+L2+H3 for both Ca-ATP and Mg-ATP. We note that these data do not exclude the possibility of the co-existing M→H2→H3. As described in the following section, at the next temperature step, where the temperature is increased by 1°C, the features of the experimental $p(r)$ were mostly governed by the presence of long polymers. The fact implies that the elongation into

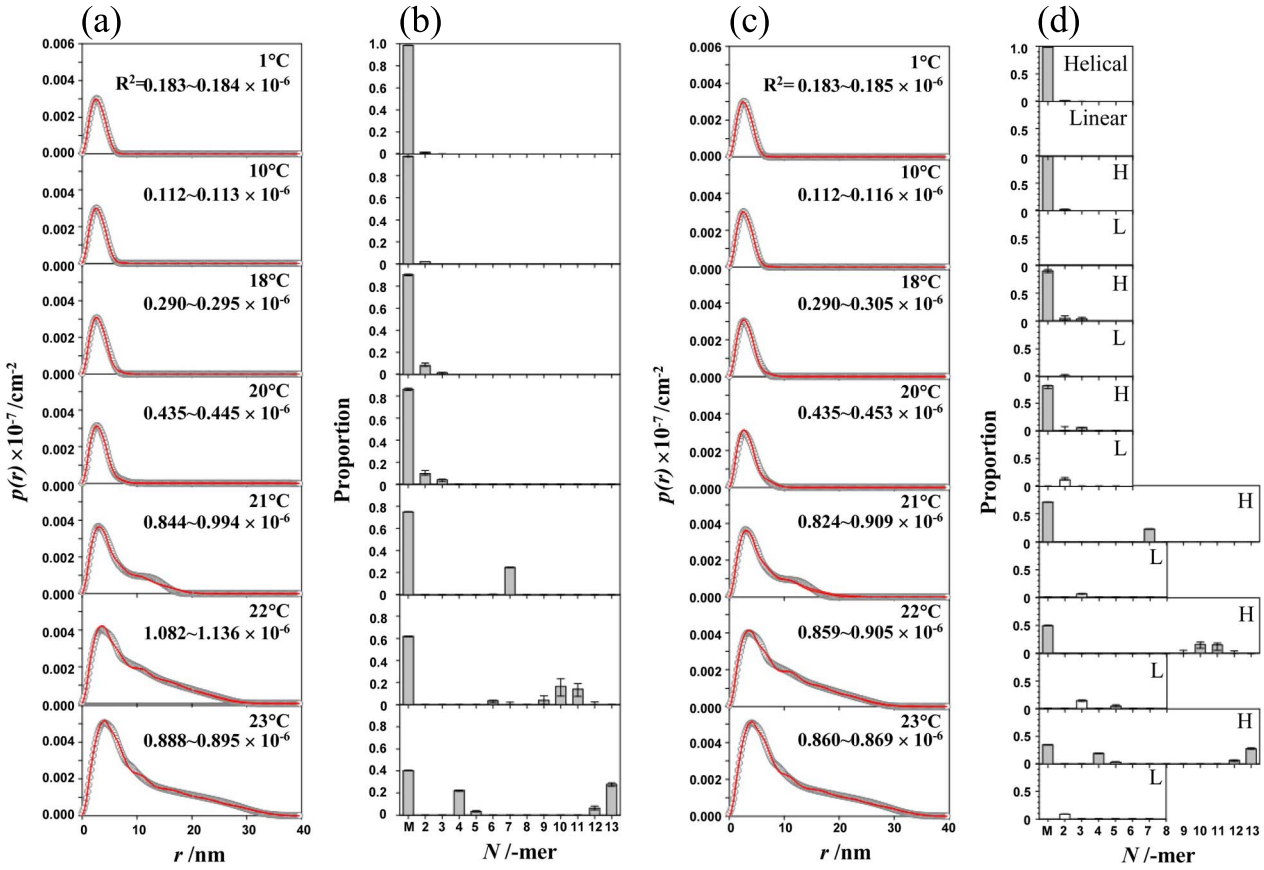

Figure 6 Evaluation of the oligomer distribution by fitting experimental $p(r)$ with the linear combination of simulated $p(r)$ for Ca-ATP-actin. (a) and (c): The experimentally obtained $p(r)$ functions (open circles) and the fitting curves (red lines) obtained by the linear combination of simulated $p(r)$s for helical (a) or linear and helical (c) oligomer models for Ca-ATP-actin. In each figure, two red lines were drawn for the range in which all the fitting results obtained from 100 trials were included. (The red lines were depicted as a single line when the two lines were very close.) The numerical values in (a) and (c) are the range of R^2 obtained by the maximum and the minimum values from 100 trials. (b) and (d): The histograms of oligomers obtained from the best-fit results using helical (b) or linear and helical (d) oligomer models, in which the error bar indicates the range between 90 percentile and 10 percentile values obtained from 100 trials.

long helical oligomers is triggered by the formation of a helical trimer (H3). The experimental scattering intensity $I(q)$ and the fitting curve using the simulated $I(q)$ from the crystallographic data were also very similar (see insets in Fig. 5a and c). This confirms that the scattering data are successfully described both in q- and real space.

Analysis of the experimental $p(r)$ profiles based on a mixture of a monomer and different oligomers calculated from the crystallographic data

We attempted to describe the experimental profiles of $p(r)$ in solution at $T^* \leq T/°C \leq T_F$ with those calculated from crystallographic data as shown in Fig. 4. Figure 6 shows that the $p(r)$ data for Ca-ATP-actin can be explained by the weighted sum of the theoretical $p(r)$ functions for a monomer and different oligomers. Figures 6a and b present the results of the fitting procedures using a monomer and helical oligomers, excluding linear oligomers, and Figs. 6c and d provide those with the mixture of monomer, helical oligomers, and the postulated linear oligomers. These results show that the simulation was not substantially improved by including the contribution of linear oligomers (judging from the value of R^2 shown in each figure), implying that the characteristic features of the experimentally obtained $p(r)$s can be interpreted as the mixture of helical oligomers and a monomer (Fig. 6b). The results of the similar analysis for Mg-ATP-actin, Ca-ADP-actin, and Mg-ADP-actin, are shown in Fig. 7 and Supplementary Figs. S2 and S3, respectively.

Almost all the analyses yielded the results, which were essentially the same as for Ca-ATP-actin. Figures 6b and 7b show that only M and small amounts of H2/L2 and H3 exist in the range of temperatures up to a certain critical temperature, as also explained in the previous section, and after the small oligomers (dimers/trimers) have been formed, the elongation appears to occur, importantly, only on the preformed oligomers. When the convergence condition of the iterative fitting algorithm was set to be larger, the distribution obtained by the fitting became broader. The case of the convergence condition set to be 10^{-2} is shown in Supplementary Fig. S1.

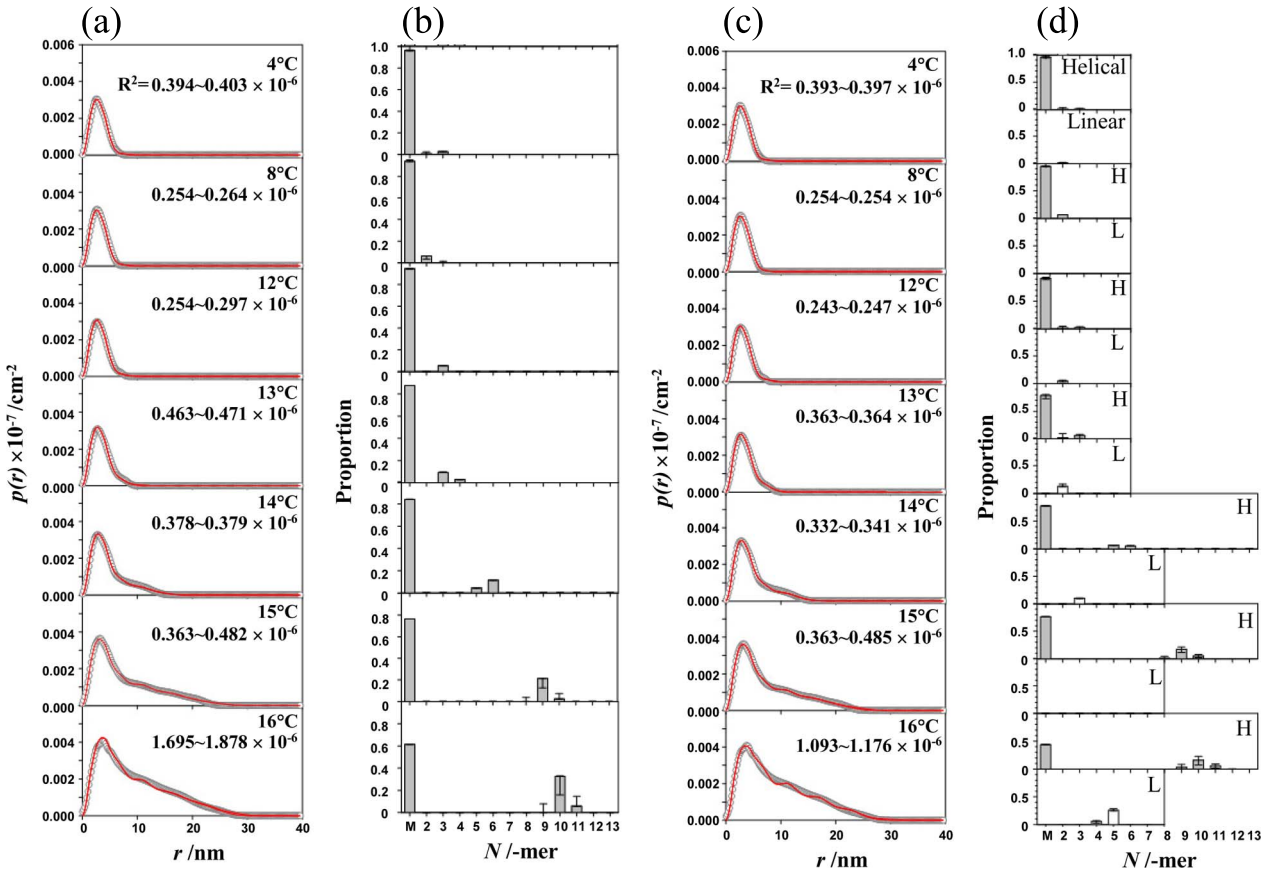

Figure 7 Evaluation of the oligomer distribution by fitting experimental $p(r)$ with the linear combination of simulated $p(r)$ for Mg-ATP-actin. (a) and (c): The experimentally obtained $p(r)$ functions (open circles) and the fitting curves (red lines) obtained by the linear combination of simulated $p(r)$s for helical (a) or linear and helical (c) oligomer models for Mg-ATP-actin. In each figure, two red lines were drawn for the range in which all the fitting results obtained from 100 trials were included. (The red lines were depicted as a single line when the two lines were very close.) The numerical values in (a) and (c) are the range of R^2 obtained by the maximum and the minimum values from 100 trials. (b) and (d): The histograms of oligomers obtained from the best-fit results using helical (b) or linear and helical (d) oligomer models, in which the error bar indicates the range between 90 percentile and 10 percentile values obtained from 100 trials.

Model-free cross-section analysis of actin oligomers

To complement the conclusion that the solutions at $T^* \le T/°C \le T_F$ were composed of a monomer and helical oligomers but not linear oligomers, we performed a virtually model-free cross-section structure analysis of actin oligomers. A simple assumption used here is that the solutions at $T^* \le T/°C \le T_F$ were the mixtures of a certain amount of monomer and elongated oligomers, letting the length and the cross-section diameter[22] be completely model-free. We applied the cross-section structure analysis to the reduced intensity $I_r(q)$ defined as

$$I_r(q) = I(q,T) - X_M I(q,T_0) \qquad (5),$$

where X_M is the monomer weight fraction.

Figure 8 displays the pair-distance distribution functions of the cross-section, $p_c(r)$, calculated from the equation (3) (see Materials and Methods), for Ca-ATP-actin at 23°C, together with $p_c(r)$ calculated for the crystal structures of helical and linear oligomers. With increasing X_M, the features of $p_c(r)$ became markedly closer to those predicted for

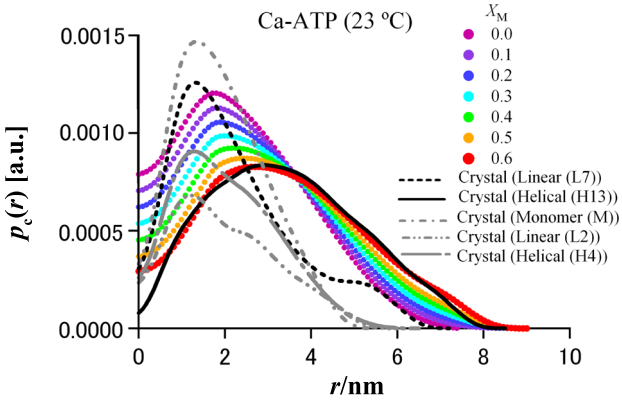

Figure 8 The model-free cross-section structure analysis of actin oligomers.

Cross-section pair-distance distribution functions $p_c(r)$ of actin oligomers for Ca-ATP at 23°C. Also shown are the simulated $p_c(r)$ for crystal structures of the elongated helical (H13) and linear (L7) aggregates. For comparison, we additionally plotted the simulated $p_c(r)$ for a monomer and short-chain oligomers, L2 and H4.

the long helical structure. When X_M=0.6 was assumed, the experimental $p_c(r)$ nicely fitted the theoretical $p_c(r)$ for H13. On the other hand, according to the fitting analysis (Fig. 6), the monomer weight fraction for Ca-ATP-actin at 23°C was ~0.4. This apparent discrepancy could be explained by the contribution from the co-existing short oligomers such as H4 (Fig. 6b). For simplicity, in this section we assumed the mixture of a monomer and a single type of a long oligomer. Therefore, if we perform the cross-section structure analysis including short oligomers like L2 and H4 (gray curves in Fig. 8) in addition to a monomer and H13 as shown in Fig. 6b, this apparent discrepancy may be eliminated.

Previous studies on the solution structure of actin oligomers at the initial stage of polymerization

As for the solution structure of actin oligomers that are formed at the initial stage of polymerization, there has been a report based on the time-resolved SAXS using synchrotron X-rays[14]. Matsudaira et al. reported that up to 60% of total actin molecules formed actin dimers just after initiating the polymerization with the addition of salts. This result is in contrast to our data, which shows that the major component is always a monomer (see Fig. 6b, d and Fig. 7b, d). This apparent contradiction may partly be due to the difference in the polymerization conditions, i.e., whether it is the addition of salts or the elevation of temperature at low ionic strength. Additionally, in the small-angle neutron scattering (SANS), the polymerization of actin was induced by quickly increasing temperature from low temperatures to 20°C, although the low-salt conditions (2 mM Tris-HCl, 1 mM ATP, 0.05 mM $MgCl_2$, 1.5 mM NaN_3, *p*D 8.4, 100 μM actin) were similar to our conditions for Mg-ATP-actin[15]. The scattering curve measured by SANS at 3 hrs after the elevation of temperature to 20°C showed that the average radius of gyration, R_g, of actin molecules was 2.9 nm. Based on the value of R_g, the authors suggested that the solution was the mixture of monomers and anti-parallel dimers. On the other hand, our results showed that the main components in Mg-ATP-actin solution at 20°C were the long polymers (see Fig. 7b, d and Fig. 3). This apparent difference may also be attributed to the difference in the polymerization conditions, i.e., using D_2O instead of H_2O as a medium and the quick increase of temperature. Also, our results were obtained not only by the estimation of the average R_g, but also by the real-space analysis of SAXS data with $p(r)$ function calculated from $I(q)$ by IFT method.

Changes in the size distribution of actin oligomers upon increasing temperature

It has been established that in the steady state the lengths of actin polymers are described by exponential distribution[7,11]. Even in the transient state, the length distribution is broad, resembling a Poisson distribution, which is explained theoretically by assuming that the binding constant of actin in the polymerization reaction does not depend on the size of polymers. On the other hand, the size distribution obtained in the present work was unexpectedly narrow and discontinuous, i.e., composed of several kinds of oligomers in addition to monomers. Once the small oligomers (dimers/trimers) are formed, the elongation appears to occur only on the preformed oligomers, maintaining the total number of oligomers nearly constant (Figs. 6b, and 7b). What is the reason for this seemingly peculiar process of polymerization? One plausible explanation for this result is that the nuclei (possibly trimers) were spontaneously formed at the temperature lower than the critical temperature T^*, and above the T^* the polymerization preferentially proceeded from the preformed nuclei, probably because the binding of actin to the nuclei was energetically more favorable than the spontaneous formation of nuclei. Thus, this unusual polymerization process may be attributed to the experimental conditions, which were unfavorable for the polymerization, so that the polymerization was forcibly induced by elevating the temperature at relatively high actin concentration (4.0 mg ml^{-1}). In any case, the present result indicates that there are multiple unique pathways for the polymerization of actin. It should be noted here that the polymerization and depolymerization dynamics of actin play an important role in various cellular functions. The existence of different pathways for actin polymerization may assist various kinds of regulatory functions of actin-associated proteins. Many important issues that should be unraveled about the dynamics of actin polymerization are still left behind.

Acknowledgments

We thank Prof. K. Kinosita, Jr. of Waseda University for his valuable suggestions on the present study. We thank Dr. S. V. Mikhailenko of Waseda University for his critical reading of the manuscript. This work was partly supported by Grants-in-Aid for Specially Promoted Research, Scientific Research (A), and "Academic Frontier" Project (S.I.), and for Young Scientists (B) and Scientific Research on Priority Areas (T. Shimozawa) from the Ministry of Education, Culture, Sports, Science and Technology (MEXT) of Japan.

REFERENCES

1. Pollard, T. D., Blanchoin, L. & Mullins, R. D. Molecular mechanisms controlling actin filament dynamics in nonmuscle cells. *Annu. Rev. Biophys. Biomol. Struct.* **29**, 545–576 (2000).
2. Carlier, M. F., Wiesner, S., Clainche, C. L. & Pantaloni, D. Actin-based motility as a self-organized system: mechanism and reconstitution *in vitro*. *C.R. Biol.* **326**, 161–170 (2003).
3. Pollard, T. D. & Borisy, G. G. Cellular motility driven by assembly and disassembly of actin filaments. *Cell* **112**, 453–465 (2003).
4. Pollard, T. D. Regulation of actin filament assembly by Arp2/3 complex and formins. *Annu. Rev. Biophys. Biomol. Struct.* **36**, 451–477 (2007).
5. Oosawa, F. & Asakura, S. *The Thermodynamics of the Polymerization of Proteins* (Academic Press, NewYork, 1975).

6. Hanson, J. & Lowy, J. The structure of actin filaments and the origin of the axial periodicity in the *I*-substance of vertebrate striated muscle. *Proc. R. Soc. Lond. B. Biol. Sci.* **160**, 449–460 (1964).
7. Kawamura, M. & Maruyama, K. Electron microscopic particle length of F-actin polymerized *in-vitro*. *J. Biochem.* **67**, 437–457 (1970).
8. Kawamura, M. & Maruyama, K. Further study of electron-microscopic particle length of F-actin polymerized *in-vitro*. *J. Biochem.* **72**, 179–188 (1972).
9. Wegner, A. Head to tail polymerization of actin. *J. Mol. Biol.* **108**, 139–150 (1976).
10. Fujiwara, I., Takahashi, S., Tadakuma, H., Funatsu, T. & Ishiwata, S. Microscopic analysis of polymerization dynamics with individual actin filaments. *Nat. Cell. Biol.* **4**, 666–673 (2002).
11. Terada, N., Shimozawa, T., Ishiwata, S. & Funatsu, T. Size distribution of linear and helical polymers in actin solution analyzed by photon counting histogram *Biophys. J.* **92**, 2162–2171 (2007).
12. Kasai, M., Asakura, S. & Oosawa, F. The cooperative nature of G-F transformation of actin. *Biochim. Biophys. Acta* **57**, 22–31 (1962).
13. Wakabayashi, K., Tokunaga, M., Kohno, I., Sugimoto, Y., Hamanaka, T., Takezawa, Y., Wakabayashi, T. & Amemiya, Y. Small-angle synchrotron x-ray scattering reveals distinct shape changes of the myosin head during hydrolysis of ATP. *Science* **258**, 443–447 (1992).
14. Matsudaira, P., Bordas, J. & Koch, M. H. J. Synchrotron x-ray diffraction studies of actin structure during polymerization. *Proc. Natl. Acad. Sci. USA* **84**, 3151–3155 (1987).
15. Goddette, D. W., Uberbacher, E. C., Bunick, G. J. & Frieden, C. Formation of actin dimers as studied by small-angle neutron-scattering. *J. Biol. Chem.* **261**, 2605–2609 (1986).
16. Rebowski, G., Boczkowska, M., Hayes, D. B., Guo, L., Irving, T. C. & Dominguez, R. X-ray scattering study of actin polymerization nuclei assembled by tandem W domains. *Proc. Natl. Acad. Sci. USA* **105**, 10785–10790 (2008).
17. Hiragi, Y., Inoue, H., Sano, Y., Kajiwara, K., Ueki, T. & Nakatani, H. Dynamic mechanism of the self-assembly process of tobacco mosaic virus protein studied by rapid temperature-jump small-angle X-ray scattering using synchrotron radiation. *J. Mol. Biol.* **213**, 495–502 (1990).
18. Mandelkow, E. M., Harmsen, A., Mandelkow, E. & Bordas, J. X-ray kinetic studies of microtubule assembly using synchrotron radiation. *Nature* **287**, 595–599 (1980).
19. Spudich, J. A. & Watt, S. The regulation of rabbit skeletal muscle contraction. I. Biochemical studies of the interaction of the tropomyosin-troponin complex with actin and the proteolytic fragments of myosin. *J. Biol. Chem.* **246**, 4866–4871 (1971).
20. Kondo, H. & Ishiwata, S. Uni-directional growth of F-actin. *J. Biochem.* **79**, 159–171 (1976).
21. Glatter, O. Computation of distance distribution functions and scattering functions of models for small angle scattering experiments. *Acta Phys. Austrica* **52**, 243–256 (1980).
22. Glatter, O. & Kratky, O. *Small-Angle X-Ray Scattering* (Academic Press, NewYork, 1982).
23. Glatter, O. Evaluation of small-angle scattering data from lamellar and cylindrical particles by the indirect Fourier transformation method. *J. Appl. Cryst.* **13**, 577–584 (1980).
24. Holmes, K. C., Popp, D., Gebhard, W. & Kabsch, W. Atomic model of the actin filament. *Nature* **347**, 44–49 (1990).
25. Otterbein, L. R., Graceffa, P. & Dominguez, R. The crystal structure of uncomplexed actin in the ADP state. *Science* **293**, 708–711 (2001).
26. Graceffa, P. & Dominguez, R. Crystal structure of monomeric actin in the ATP state. Structural basis of nucleotide-dependent actin dynamics. *J. Biol. Chem.* **278**, 34172–34180 (2003).
27. Oda, T., Iwasa, M., Aihara, T., Maeda, Y. & Narita, A. The nature of the globular- to fibrous-actin transition. *Nature* **457**, 441–445 (2009).
28. Kasai, M. & Oosawa, F. Behavior of divalent cations and nucleotides bound to F-actin. *Biochim. Biophys. Acta* **172**, 300–310 (1969).
29. Selden, L. A., Estes, J. E. & Gershman, L. C. The tightly bound divalent cation regulates actin polymerization. *Biochem. Biophys. Res. Commun.* **116**, 478–485 (1983).
30. Gershman, L. C., Newman, J., Selden, L. A. & Estes, J. E. Bound-cation exchange affects the lag phase in actin polymerization. *Biochemistry* **23**, 2199–2203 (1984).
31. Pollard, T. D. Rate constants for the reactions of ATP- and ADP-actin with the ends of actin filaments. *J. Cell. Biol.* **103**, 2747–2754 (1986).
32. Sato, T., Komatsu, T., Nakagawa, A. & Tsuchida, E. Induced long-range attractive potentials of human serum albumin by ligand binding. *Phys. Rev. Lett.* **98**, 208101–208104 (2007).